Revisiting the Tropical Atlantic Influence on El Niño-Southern Oscillation

Richter, Ingo
Application Laboratory, Research Institute for Value-Added-Information Generation, Japan Agency for Marine-Earth Science and Technology

Tokinaga, Hiroki
Research Institute for Applied Mechanics, Kyushu University

Kosaka, Yu
Research Center for Advanced Science and Technology, University of Tokyo

Doi, Takeshi
Application Laboratory, Research Institute for Value-Added-Information Generation, Japan Agency for Marine-Earth Science and Technology

他

出版情報：Journal of Climate. 34 (21), pp.8533-8548, 2021-11-01. American Meteorological Society
バージョン：

Revisiting the Tropical Atlantic Influence on El Niño–Southern Oscillation

INGO RICHTER,[a] HIROKI TOKINAGA,[b] YU KOSAKA,[c] TAKESHI DOI,[a] AND TAKAHITO KATAOKA[d]

[a] *Application Laboratory, Research Institute for Value-Added-Information Generation, Japan Agency for Marine-Earth Science and Technology, Yokohama, Japan*
[b] *Research Institute for Applied Mechanics, Kyushu University, Kasuga, Japan*
[c] *Research Center for Advanced Science and Technology, University of Tokyo, Tokyo, Japan*
[d] *Research Center for Environmental Modeling and Application, Japan Agency for Marine-Earth Science and Technology, Yokohama, Japan*

(Manuscript received 29 January 2021, in final form 24 July 2021)

ABSTRACT: The influence of the tropical Atlantic on El Niño–Southern Oscillation (ENSO) is examined using sensitivity experiments with the SINTEX-F general circulation model with prescribed sea surface temperature (SST) distributions based on observations for the period 1982–2018. In the control experiment (CTRL) observed SSTs are prescribed over the global oceans; in the sensitivity experiment observed SSTs are prescribed in the tropical Atlantic only, while in other regions the climatological annual cycle is prescribed. A composite analysis of the model output suggests that cold SST events in the northern tropical Atlantic during boreal spring are associated with near-surface wind changes over the equatorial and subtropical Pacific that are conducive to the development of El Niño, consistent with previous studies. The amplitude of these changes, however, is at most 20% of those observed during typical El Niño events. Likewise, warm events in the equatorial Atlantic produce only about 10% of the wind changes seen in the western equatorial Pacific during the developing phase of typical La Niña events. Similar results are obtained from a partial regression analysis performed on an ensemble of atmosphere-only simulations from phase 6 of the Atmospheric Model Intercomparison Project (AMIP) although the equatorial Atlantic influence is stronger in AMIP. Further analysis of the AMIP models indicates that model biases do not have a major impact on the Atlantic-to-Pacific influence. Overall, the results suggest that the tropical Atlantic has a rather weak influence on ENSO development and mostly acts to modulate ongoing events rather than initiate them.

SIGNIFICANCE STATEMENT: Previous work has suggested that year-to-year surface temperature variations in the tropical Atlantic can contribute to the development of so-called El Niño events, which are warm events in the equatorial Pacific with global impacts on climate and weather extremes. Here we use experiments with a global climate model as well as archived climate model simulations to quantify the tropical Atlantic influence and its importance for El Niño development. Our results suggest that the Atlantic can at most contribute 10%–20% to the development of El Niño, and that it should be seen more as modulating El Niño rather than initiating it. After accounting for different methodologies, our estimates are consistent with those of previous studies.

KEYWORDS: Atlantic Ocean; ENSO; Teleconnections; Interannual variability

1. Introduction

It has long been known that the northern tropical Atlantic (NTA) is strongly influenced by El Niño–Southern Oscillation (ENSO) in late boreal winter and early spring [Covey and Hastenrath 1978; Curtis and Hastenrath 1995; Enfield and Mayer 1997; Klein et al. 1999; Saravanan and Chang 2000; Alexander et al. 2002; see also reviews by Cai et al. (2019) and Wang (2019)]. During the mature and decaying phases of El Niño events, warm sea surface temperatures (SSTs) in the eastern tropical Pacific cause changes in surface heat fluxes that are conducive to warming in the NTA. More specifically, cooling through surface latent heat flux is reduced while warming through downward shortwave radiation is increased. Several mechanisms contribute to this influence: a weakening of the NTA trade winds due to extratropical influences via the Pacific–North American pattern (Wallace and Gutzler 1981; Lee et al. 2008) and tropical influences via the Walker and Hadley circulations (Klein et al. 1999; Saravanan and Chang 2000; Wang 2002; Huang 2004; Sasaki et al. 2014), as well as El Niño–induced upper tropospheric warming that stabilizes the atmosphere over the NTA and thus suppresses cloud formation (Klein et al. 1999; Chiang and Sobel 2002).

More recently, it has been suggested that the NTA itself can change the course of ENSO (Ham et al. 2013a,b; Ding et al. 2017; Wang et al. 2017). SST anomalies in the NTA occur on interannual to decadal time scales and are associated with the so-called Atlantic meridional mode (AMM) of variability (Hastenrath and Heller 1977; Xie 1996; Chang et al. 1997; Amaya et al. 2017). Ham et al. (2013a, hereafter H13) suggest

Denotes content that is immediately available upon publication as open access.

Supplemental information related to this paper is available at the Journals Online website: https://doi.org/10.1175/JCLI-D-21-0088.s1.

Corresponding author: Ingo Richter, richter@jamstec.go.jp

DOI: 10.1175/JCLI-D-21-0088.1

that a warm event in the NTA during late winter forces an atmospheric Rossby wave response to the west, which is associated with anomalously low pressure over the subtropical northeast Pacific. The cyclonic flow on the western flank of this anomalous low enhances the northeast trade winds and subsequently generates cool SST anomalies to the west. As these cool SST anomalies strengthen in boreal spring, they engender easterly wind anomalies over the western equatorial Pacific that contribute to the development of La Niña–like SST anomalies (the so-called La Niña Modoki; Ashok et al. 2007).

An interesting aspect of the NTA-to-ENSO mechanism is that it suggests a *negative* correlation between SST anomalies in the NTA and those in the tropical Pacific. This is in contrast to the ENSO-to-NTA mechanism, which suggests a *positive* correlation between SST anomalies in the two regions. This would be consistent with the following chain of events: a decaying El Niño event forces warm SST anomalies in the NTA, which in turn contribute to subsequent cooling in the tropical Pacific. In this sense, El Niño would shorten its own duration via the NTA feedback. Some idealized modeling studies have indeed found that, in the absence of tropical Atlantic SST variability, the power spectrum of equatorial Pacific SSTs shifts toward longer periods (Dommenget et al. 2006). Similar results were obtained by Wang et al. (2017) using observations and a general circulation model (GCM).

In addition to the NTA, there has also been recent interest in the equatorial Atlantic influence on ENSO. SST variability in the equatorial Atlantic occurs on interannual time scales and is associated with the Atlantic zonal mode (AZM), also known as the Atlantic Niño [see reviews by Lübbecke et al. (2018), Cabos et al. (2019), and Richter and Tokinaga (2021)]. The AZM typically develops in boreal spring and peaks in summer. A number of previous studies have examined the influence of ENSO on the AZM and have found it to be inconsistent (Chang et al. 2006; Lübbecke and McPhaden 2012), with only some ENSO events followed by AZM events of the opposite sign (Vallès-Casanova et al. 2020) and, notably, the 1982/83 and 1997/98 major El Niño events followed by negative and positive AZM events, respectively (Chang et al. 2006). Regarding the AZM-to-ENSO influence, several studies suggest that the AZM can change the equatorial Walker circulation in such a way as to cause (or contribute to) opposite-signed ENSO events in the following winter (Wang 2006; Jansen et al. 2009; Rodríguez-Fonseca et al. 2009; Frauen and Dommenget 2012; Ding et al. 2012; Kucharski et al. 2011, 2015; Polo et al. 2015; Chikamoto et al. 2020).

A potential problem in disentangling the two-way basin interactions is that all variability patterns involved (ENSO, AMM, and AZM) tend to develop in boreal spring, making it difficult to assign causality. An incipient ENSO event, for instance, may be the cause or the consequence of an incipient AZM event. Furthermore, ENSO events are often followed by opposite-signed events in the next year (particularly in the case of positive events). Accordingly, a decaying El Niño event will cause warming in the NTA during the following spring but the ensuing La Niña event may merely be due to ENSO's intrinsic phase reversal rather than the NTA influence. This argument has been investigated in a recent study by Zhang et al. (2021), who come to the conclusion that the influence of the NTA on ENSO is spurious and consistent with the null hypothesis of ENSO autocorrelation. Resolving these issues based on observations is difficult because the observational record is relatively short. Climate model simulations can overcome the problem of short time series but are subject to model biases, which include an erroneous southward displacement of the Atlantic intertropical convergence zone (ITCZ; e.g., Doi et al. 2012; Richter et al. 2014; Richter and Tokinaga 2020), and poor phase locking of ENSO variability (e.g., Bellenger et al. 2014). Such biases may lead to erroneous estimates of the strength of the tropical Atlantic influence on ENSO.

In the light of these potential problems, it is important to further examine the linkage between tropical Atlantic variability and ENSO. To this end, the present study examines observations, an ensemble of atmosphere-only simulations from phase 6 of the Coupled Model Intercomparison Project (CMIP6), and dedicated sensitivity tests with the SINTEX-F GCM. These datasets and the methodology will be described in section 2. The results of the SINTEX-F sensitivity tests will be examined in section 3, while the multimodel analysis is presented in section 4. Section 5 is devoted to examining how GCM biases influence the link between the tropical Atlantic and ENSO. In section 6 we discuss the relative importance of the Atlantic influence and try to reconcile our results with those of previous studies. A summary and conclusions are given in section 7.

2. Data and methods

a. Model description

We use the SINTEX-F GCM to conduct sensitivity tests with prescribed SST distributions. The model was developed under a European Union–Japan collaboration project (Luo et al. 2003, 2005) and is based on the European SINTEX model (Gualdi et al. 2003). The version used here consists of the ECHAM 4.6 AGCM (Roeckner et al. 1996), the OPA 8.2 oceanic GCM (OGCM; Madec et al. 1998), and the OASIS 2.4 coupler (Valcke et al. 2000). The atmospheric resolution is T106 (approximately 1.1°), with 19 vertical levels, four or five of which are inside the planetary boundary layer. The oceanic resolution is 2° × 2° with the meridional resolution increasing to 0.5° at the equator. The OGCM has 31 vertical levels, 19 of which lie within the top 400 m.

To achieve the desired SST distributions strong SST restoring (1-day time scale) is used, resulting in SST boundary conditions that are very similar to an Atmospheric Model Intercomparison Project (AMIP)-type simulation but may differ from the imposed SST distribution by about 0.1 K. Thus, while the model is run with both atmospheric and oceanic components active, SSTs can essentially not react to the atmospheric forcing, leading to an almost complete decoupling of atmosphere and ocean. The original motivation for the decoupling approach was to use the ocean state of these experiments for future coupled sensitivity tests.

Several experiments are conducted (see Table 1), each consisting of nine ensemble members, which are generated by perturbing the SST boundary conditions with random values of

TABLE 1. SINTEX-F sensitivity experiments examined in this study. All experiments were performed with strong SST restoring for the period 1982–2014. SSTs and their monthly climatology were derived from the OISST observations for the same period.

Experiment name	Description
CTRL	Observed SST everywhere
OTA	Observed SST in the tropical Atlantic, climatology elsewhere
CGL	Climatology globally
TAbias	Observed SSTA added to monthly climatology derived from free-running coupled SINTEX-F simulation in the tropical Atlantic

amplitude 0.01 K. In the control experiment (CTRL) SSTs are restored to the Optimally Interpolated SST (OISST; Reynolds et al. 2002) observations from 1982 to 2014.

In another experiment, called OTA (for observed tropical Atlantic), observed SSTs are prescribed in the tropical Atlantic (from 30°S to 30°N) only, while the observed climatological annual cycle is prescribed elsewhere. Thus, OTA has nonzero SST anomalies in the tropical Atlantic only. This experiment serves to isolate the remote influences of the tropical Atlantic. The prescribed climatology is derived from the 1982–2014 OISST observations. Meridional transition zones of 5° are used to gradually blend climatological and interannually varying SSTs at the northern and southern edges of the tropical Atlantic.

In an additional experiment, called CGL (for global climatology), SSTs are restored to climatology globally. Variability in this experiment should be entirely due to atmospheric internal variability. This allows checking composites and correlations against the null hypothesis of internal variability. More information on CTRL and CGL can be found in Richter and Doi (2019).

In a further experiment, TAbias (for tropical Atlantic bias), we examine the impact of tropical Atlantic biases by adding the observed (OISST) tropical Atlantic SST anomalies to the monthly climatology of a 500-yr free-running coupled control simulation of SINTEX-F. Thus, the SST anomalies are as observed, but the annual cycle is that of the free-running SINTEX-F. This experiment was originally performed to investigate the impact of biases on the simulation of variability over the tropical Atlantic itself (Richter et al. 2018).

For each experiment, anomalies are calculated as deviations from the monthly climatological cycle for the period 1982–2014, with the linear trend removed.

b. *Reanalysis and observational data*

Our reference data for SST and atmospheric fields are the European Centre for Medium-Range Weather Forecasts (ECMWF) reanalysis 5 (ERA5; Hersbach et al. 2018) for the period 1979–2018. For precipitation, we also make use of the Global Precipitation Climatology Project (GPCP) version 2.3 (Adler et al. 2003).

c. *AMIP simulations*

We analyze simulations from the AMIP experiment, which is part of CMIP6. In this experiment, atmospheric GCMs are run in atmosphere-only mode with observed SST forcing for the period 1979–2014. A list of all the 24 models examined is given in Table 2. For the AMIP simulations as well as for the observations, anomalies are calculated in the same manner as for the SINTEX-F experiments.

d. *Methods*

1) COMPOSITES

The sensitivity tests with the SINTEX-F GCM form the core of this study. By comparing experiments CTRL and OTA, we can estimate the influence of tropical Atlantic SST anomalies on atmospheric circulation anomalies over the Pacific. To do this, we composite fields on cold events in the NTA and on warm events in the ATL3 region. Cold events in the NTA (NTA−) are chosen based on the February–April (FMA) mean of the NTA index (SSTs averaged over the region 40°–10°W, 10°–20°N; box indicated in Fig. 1a) being below −0.8 standard deviations. This criterion selects the years 1985, 1986, 1989, 1994, 1999, 2003, 2009, 2012, and 2014. Warm events in the ATL3 (AZM+) are chosen based on the June–August (JJA) mean of the ATL3 index (SSTs averaged over the region 20°–0°W, 3°S–3°N) exceeding 0.8 standard deviations. For AZM+, the years 1984, 1987, 1988, 1995, 1996, 1998, 1999, and 2008 are selected. The composite years are the same for both CTRL and OTA. The polarity of events is chosen such that it has a stronger response in the Pacific target region.

2) PARTIAL REGRESSION ANALYSIS

Even though the SINTEX-F sensitivity experiments are a useful tool, there is some uncertainty due to model biases. It is therefore desirable to compare with other models in order to confirm the robustness of the results. While we cannot perform sensitivity experiments with the AMIP models, we can subject them to a partial regression analysis, as done for observations by H13. Their approach was to remove the influence of ENSO by regressing out the preceding December–February (DJF) Niño-3.4 index (SSTs averaged over 170°–120°W, 5°S–5°N) from all analysis fields. They then regressed the residual fields on SST averaged over the northern tropical Atlantic (0°–15°N, 80°W–20°E), focusing in particular on the following March–May (MAM) season. These partial regressions were assumed to represent the influence of the northern tropical Atlantic on the tropical Pacific. We note that their definition of the NTA covers a larger area than ours and that it encompasses the equatorial Atlantic as well. In the present study we would like to separate the equatorial and northern tropical Atlantic influences and therefore choose the more confined NTA area. Other than that, we follow the approach by H13 for our analysis of the northern tropical Atlantic influence. For the equatorial Atlantic, we slightly modify the procedure by regressing out the contemporaneous Niño-3.4 index. This is done because, for the equatorial Atlantic, we are interested in JJA, when the influence of the preceding winter is not very strong. The sensitivity of our results to the details of the partial regression method is explored in some more detail in section 2 of the online supplemental material.

We also perform these regression analyses on the SINTEX-F CTRL experiment. This allows us to compare how well the

TABLE 2. The CMIP6 AMIP models used in this study (letter labels are used in Fig. 6).

Model name	Label	Nation	Atmospheric component and resolution
BCC-CSM2-MR	c	China	BCC_AGCM3_MR; T106 (~1.125° × 1.125°); 46 levels
BCC-ESM1	d	China	BCC_AGCM3_LR; T42 (~2.8125° × 2.8125°); 26 levels
CAMS-CSM1-0	e	China	ECHAM5_CAMS; T106 (~1.125° × 1.125°); 31 levels
CanESM5	f	Canada	CanAM5; T63 linear Gaussian grid (~2.8125° × 2.8125°); 49 levels
CESM2-WACCM	g	United States	CAM6; Finite volume grid (0.9° × 1.25°); 70 levels
CESM2	h	United States	CAM6; Finite volume grid (0.9° × 1.25°); 32 levels
CNRM-CM6-1	i	France	ARPEGE 6.3; T127 (~100 km); 91 levels
CNRM-ESM2-1	j	France	ARPEGE 6.3; T127 (~100 km); 91 levels
E3SM-1-0	k	United States	EAM v1.0; 1° average grid spacing; 72 levels
EC-Earth3-Veg	l	European countries	IFS cy36r4; TL255 (~70 km); 91 levels
EC-Earth3	m	European countries	IFS cy36r4; TL255 (~70 km); 91 levels
FGOALS-f3-L	n	China	FAMIL2.2; C96 (~1° × 1°); 32 levels
FGOALS-g3	o	China	GAMIL2; 180 × 90 (~200 km); 26 levels
GISS-E2–1-G	p	United States	GISS-E2.1; 2.5° × 2°; 40 levels
HadGEM3-GC31-LL	q	United Kingdom	MetUM-HadGEM3-GA7.1; N96 (1.875° × 1.25°); 85 levels
HadGEM3-GC31-MM	r	United Kingdom	MetUM-HadGEM3-GA7.1; N216 (~0.83° × 0.55°); 85 levels
IPSL-CM6A-LR	s	France	LMDZ; N96 (2.5° × 1.259°); 79 levels
MIROC6	t	Japan	CCSR AGCM; T85 (~1.4° × 1.4°); 81 levels
MRI-ESM2-0	u	Japan	MRI-AGCM3.5; TL159 (~120 km); 80 levels
NESM3	v	China	ECHAM v6.3; T63 (1.9° × 1.9°); 47 levels
NorCPM1	w	Norway	CAM-OSLO4.1; ~2.5° × 2°; 26 levels
NorESM2-LM	x	Norway	CAM-OSLO; ~2.5° × 2°; 32 levels
SAM0-UNICON	y	South Korea	CAM5.3 with UNICON; ~1° × 1°; 30 levels
UKESM1-0-LL	z	United Kingdom	MetUM-HadGEM3-GA7.1; N96 (1.875° × 1.25°); 85 levels

results from the OTA sensitivity experiment agree with the partial regression results. We explain the comparison method for one particular example, the influence of the NTA on 10-m zonal wind anomalies area-averaged over the far western Pacific (FWP; 5°S–5°N, 140°–170°E) region. The partial regression performed on CTRL gives us a sensitivity estimate in meters per second per kelvin ($m\,s^{-1}\,K^{-1}$); that is, it tells us the wind anomaly ($m\,s^{-1}$) in the FWP for a given SST anomaly (K) in the NTA. For comparison, we take the NTA− composites (see above in this section) for experiment OTA and divide the FWP 10-m zonal wind anomaly by the NTA SST anomaly. To the extent that the partial regression method in CTRL agrees with the composite method in OTA, we have confidence that it provides an alternative way of quantifying remote influences that can also be applied to AMIP simulations and the ERA5 reanalysis. Having a multimodel comparison, in turn, allows us to evaluate the influence of model biases on teleconnections.

3) REGIONS OF INTEREST

To investigate the influence of the tropical Atlantic on the Pacific, several regions are of particular interest. The FWP region comprises the area of strongest zonal wind variability and is of interest for studying the initial forcing of ENSO events. The subtropical North Pacific is thought to be a region where the precursors of some ENSO events occur, particularly those of the Modoki type (e.g., Amaya 2019). H13 argued that the NTA influence on the tropical Pacific is mediated by sea level pressure (SLP), surface wind, and latent heat flux anomalies in this general region. These precursors are also linked to the Pacific meridional mode (Chiang and Vimont 2004). To measure wind speed anomalies associated with the NTA influence, we define a subtropical northeast Pacific (SNEP) index as the average over the region 10°–30°N, 150°–110°W. Our subsequent analysis revealed significant SLP anomalies to the north, in the region of the Aleutian low (AL), which motivated the definition of an AL index (SLP averaged over 30°–60°N, 180°–120°W). Finally, we also examine zonal wind anomalies in the far eastern Pacific (FEP; defined as ocean points in 5°–15°N, 110°–90°W).

3. SINTEX-F sensitivity tests

We begin our analysis by analyzing the unstratified pointwise correlation of experiments OTA and CTRL (Fig. 1). This gives a first impression of the global influence of tropical Atlantic SST anomalies. Zonal wind anomalies are of particular interest as they are crucial to ENSO development but also indicative of wind speed anomalies in off-equatorial regions. Here we show the zonal wind at 850 hPa (Fig. 1a), rather than the 10-m wind anomalies, to rule out excessive influence by the fixed surface temperatures. Further analysis does not show a strong influence of the analysis level on the estimation of the remote impacts (see Fig. S6 in the online supplemental material). Correlations above 0.6 appear over the equatorial Atlantic and the Western Hemisphere warm pool (WHWP). The high correlation over the equatorial Atlantic is expected due to the relatively strong influence of the zonal SST gradient on zonal winds in the region. The high correlation over the WHWP is likely due to the influence of the prescribed SST anomalies on convective activity in the region, which is closely related with the low-level winds. Elsewhere, including in the

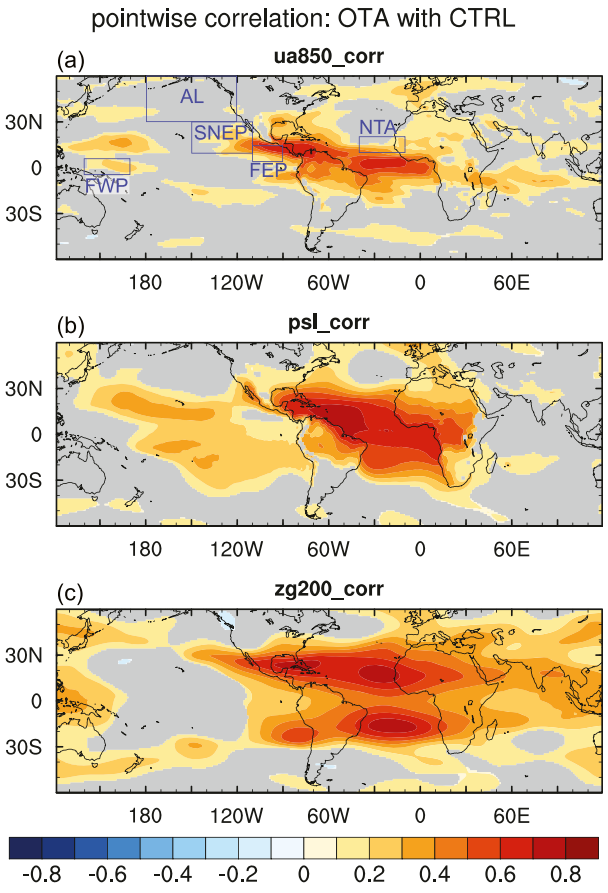

FIG. 1. Pointwise correlation of the SINTEX-F experiments OTA (observed SST in the tropical Atlantic, climatology elsewhere) with CTRL (observed SST globally) for (a) 850-hPa zonal wind, (b) SLP, and (c) 200-hPa geopotential height. Values significant at the 95% level are shaded. The blue boxes in (a) show target regions used for area averages (see section 2d).

NTA region, the extratropical Atlantic, and the equatorial Pacific, the correlation coefficients are small and often fail the significance test, suggesting a relatively weak influence of the tropical Atlantic SST on the low-level winds. Repeating the correlation analysis with the 10-m zonal wind yields very similar results (not shown). We will therefore focus on the latter field in our analysis.

SLP gives an integrative measure of the general circulation. For this field, correlations are above 0.5 over most of the tropical Atlantic (Fig. 1b). Over the tropical Pacific, values are around 0.2–0.3, while over the tropical Indian Ocean they are close to zero.

The 200-hPa geopotential height is useful for examining the far-field response to convection anomalies over the tropical Atlantic. High correlations straddle the equatorial Atlantic in the subtropics of both hemispheres (Fig. 1c). These protrude into the far eastern Pacific but drop below significance farther west. Relatively high values are also found to the east of the tropical Atlantic, where they tend to be more centered on the equator and protrude toward the Pacific warm pool. The global pattern has a remote similarity with the Matsuno–Gill pattern (Matsuno 1966; Gill 1980), with its forcing region centered in the eastern equatorial Atlantic.

We examine the NTA− and AZM+ composites (Fig. 2). In the NTA region, 10-m wind speed anomalies in the reanalysis have their highest positive values in January (Fig. 2a), indicating increased upward latent heat flux and a deepening of the oceanic mixed layer (Kataoka et al. 2019), which result in oceanic cooling. CTRL reproduces the peak in January, albeit at much weaker amplitude, which may be due to a relatively strong atmosphere-to-ocean forcing in the region; that is, the observed NTA SST anomalies are in part due to internal atmospheric variability, which is not constrained by the prescribed SST in our experiments. Additionally, the reanalysis represents a single realization while CTRL is a nine-member ensemble average.

In contrast to CTRL, the NTA wind speed anomalies in OTA are close to zero and indistinguishable from the CGL experiment, which suggests that the wind anomalies in the NTA are mostly controlled from outside the tropical Atlantic. This is consistent with the finding of Richter and Doi (2019) that the tropical Pacific has the strongest influence on NTA wind anomalies.

In the FWP (Fig. 2b), 10-m zonal wind in OTA is weak but consistently westerly ($\sim$0.2 m s^{-1}). This is in contrast to the easterly anomalies in CTRL and ERA5, which are due to the La Niña events that typically precede NTA− events. Opposite-signed fields in CTRL and OTA can also be seen for 10-m wind speed in the SNEP (Fig. 2c) and for SLP in the AL (Fig. 2d; see also Fig. S7 and the discussion in the online supplemental material). The former, however, is relatively weak (from −0.2 to 0.2 m s^{-1}) and only significant in January and February. The opposite signs of wind anomalies in CTRL and OTA suggest that the tropical Atlantic SST anomalies, by themselves, act to accelerate the decay of the preceding La Niña event, consistent with Dommenget et al. (2006) and Wang et al. (2017).

Other anomaly fields in the NTA− composites of OTA are weak over the entire Pacific from January through April, with only a hint of westerly anomalies in the far western equatorial Pacific. We note that the evolution of the Pacific anomalies in CTRL agrees reasonably well with those in the ERA5 reanalysis (Figs. S1 and S2).

Inspection of Figs. 1 and 3 suggests a westward influence of the NTA on the Pacific (high correlations of SLP and 200-hPa geopotential in Fig. 1), presumably through a Matsuno–Gill response to the west. The cool SST anomalies in the NTA (Fig. 3) are accompanied by a southward shift of the Atlantic ITCZ (not shown), with convective anomalies both north and south of the equator. The westward pathway in the Northern and Southern Hemispheres is partly consistent with what has been reported by H13 and Wang et al. (2010). An eastward pathway through extratropical Rossby wave trains, however, cannot be ruled out, as high correlations are seen in the 200-hPa height field (Fig. 1c). Regardless of the pathway, it is clear that the western Pacific responds with an analogous southward shift of the ITCZ, which is accompanied by northwesterly wind anomalies in the region.

For the AZM+ composites (Fig. 2e), FWP zonal wind anomalies in CTRL are easterly, consistent with the moderate La Niña conditions that develop toward the end of the year (not shown). OTA also features easterly anomalies, but these are only about −0.1 m s^{-1} during boreal summer when the

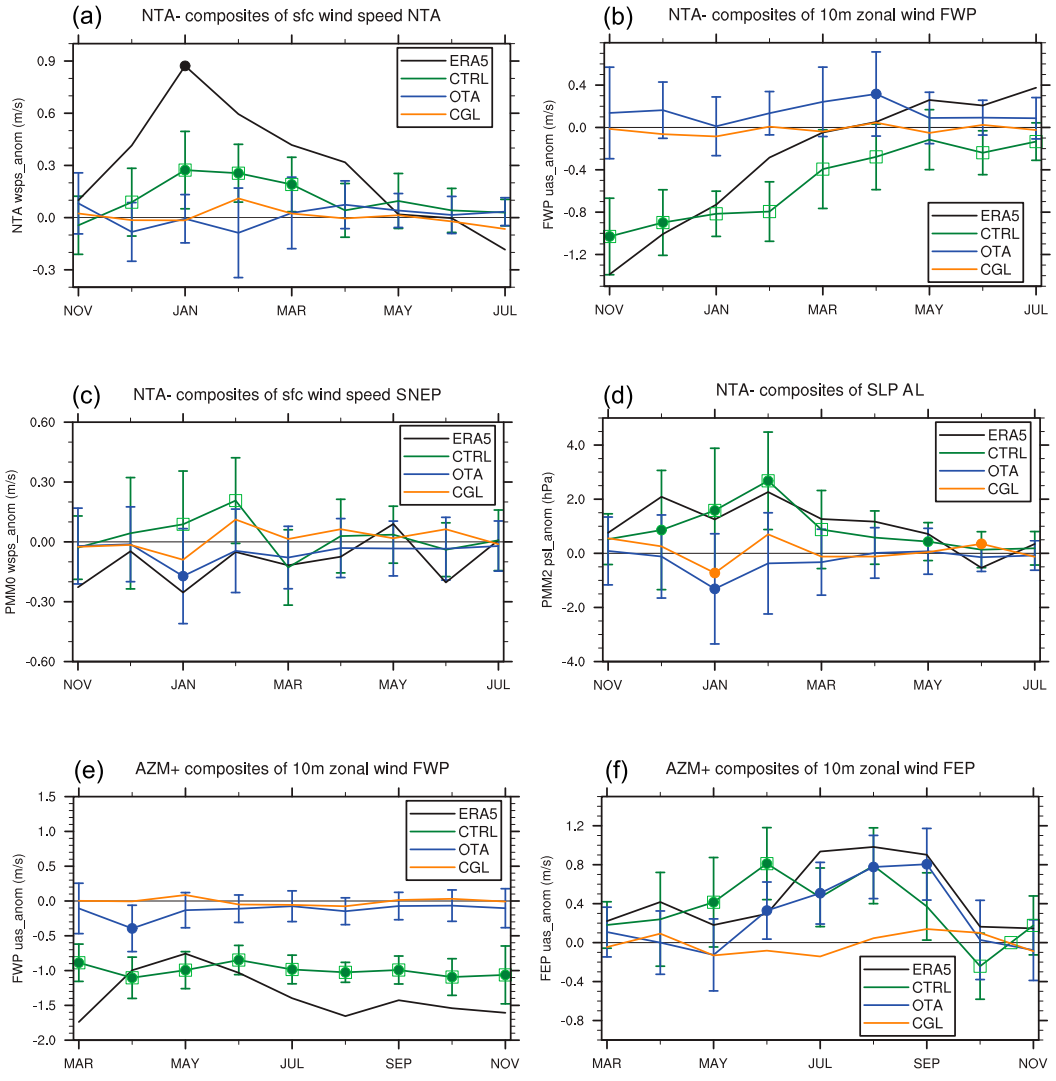

FIG. 2. Composite anomalies for ERA5 (black line), CTRL (green line), OTA (blue line), and CGL (orange line). The individual panels show (a) 10-m wind speed in the NTA during cold NTA events, (b) 10-m zonal wind in the FWP during cold NTA events, (c) 10-m wind speed in the SNEP during cold NTA events, (d) SLP in the AL during cold NTA events, (e) 10-m zonal wind in the FWP during warm AZM events, and (f) 10-m zonal wind in the FEP during warm AZM events. Values significantly different from zero at the 95% level are marked with filled circles. Values in CTRL that are significantly different from OTA at the 95% level are marked with green boxes. The error bars for CTRL and OTA indicate the standard deviation across events and ensemble members.

AZM is most pronounced. The AZM influence on western equatorial Pacific surface winds is somewhat stronger in boreal spring, with $-0.4\,\mathrm{m\,s^{-1}}$ in April. This may be related to both the Pacific and the Atlantic ITCZ being close to the equator in spring (Tokinaga et al. 2019), which provides ideal conditions for equatorial Atlantic SST anomalies to influence deep convection and the Walker circulation. We note that the wind anomalies in CTRL are quite steady throughout the analysis period, indicating that they are related to processes that evolve more slowly than the relatively short-lived AZM.

The situation is different in the far eastern Pacific (FEP region; Fig. 2f). Here, the zonal wind anomalies show a roughly similar evolution and amplitude in OTA and CTRL, suggesting a strong equatorial Atlantic influence. We note that wind anomalies develop later and have a stronger amplitude in ERA5 than in CTRL.

We examine the horizontal maps of AZM+ composites (Fig. 4). A comparison of CTRL with ERA5 composites (Figs. S1 and S3) suggests that the model successfully reproduces many of the large-scale features, including easterly and westerly zonal wind anomalies in the western and eastern equatorial Pacific, respectively. OTA mostly shows weak anomalies in the Pacific. Two exceptions are westerly anomalies in the far eastern Pacific during summer, and easterly anomalies in the far western Pacific during April. The latter wind anomalies extend into the southern tropical

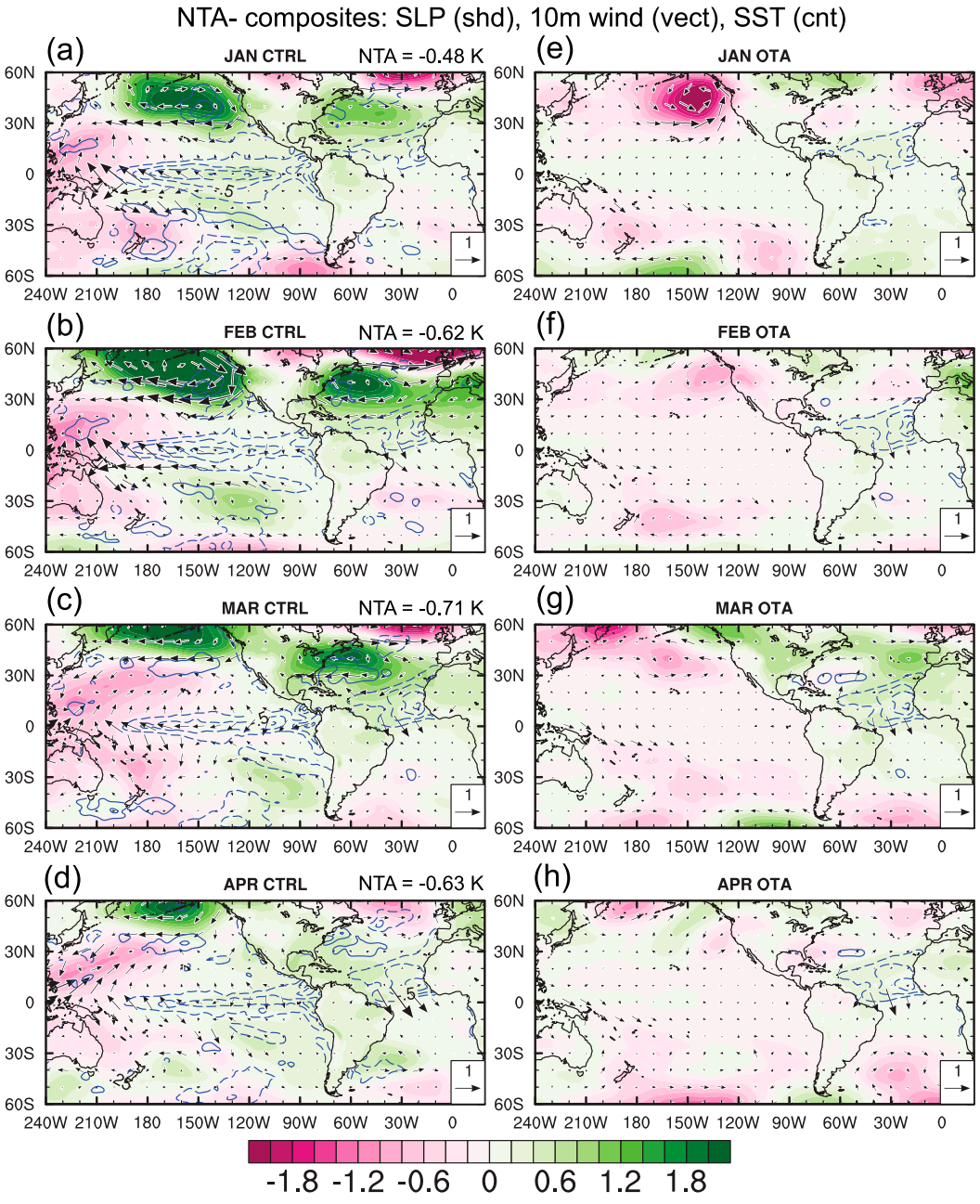

FIG. 3. Anomalies of SLP (shading; hPa), 10-m wind (vectors; reference 1 m s^{-1}), and SST (blue contours; contour interval 0.25 K; zero contour omitted; negative contours dashed) composited on cold NTA events, shown for (left) CTRL and (right) OTA. The value of the NTA index is shown on the right above each panel for CTRL.

Pacific but are absent in the Northern Hemisphere. This meridional asymmetry resembles the one in the NTA− composites and suggests a similar pathway.

4. Partial regression analysis and comparison with the AMIP models

We use the partial regression method described in section 2 to estimate remote influences of the NTA and ATL3 on the Pacific atmospheric circulation. We start by applying the method to the SINTEX-F CTRL simulation (Fig. 5b) and compare with the results from the CTRL and OTA composites for NTA− (Fig. 3). The partial regression successfully reproduces some salient features of OTA. Most notably, it shows the reversal of the 10-m wind anomalies over the far western equatorial Pacific; that is, winds are weakly westerly in the partial regression (Fig. 5b) and OTA (Fig. 3, right) but easterly in CTRL (Fig. 3, left). The partial regression also successfully

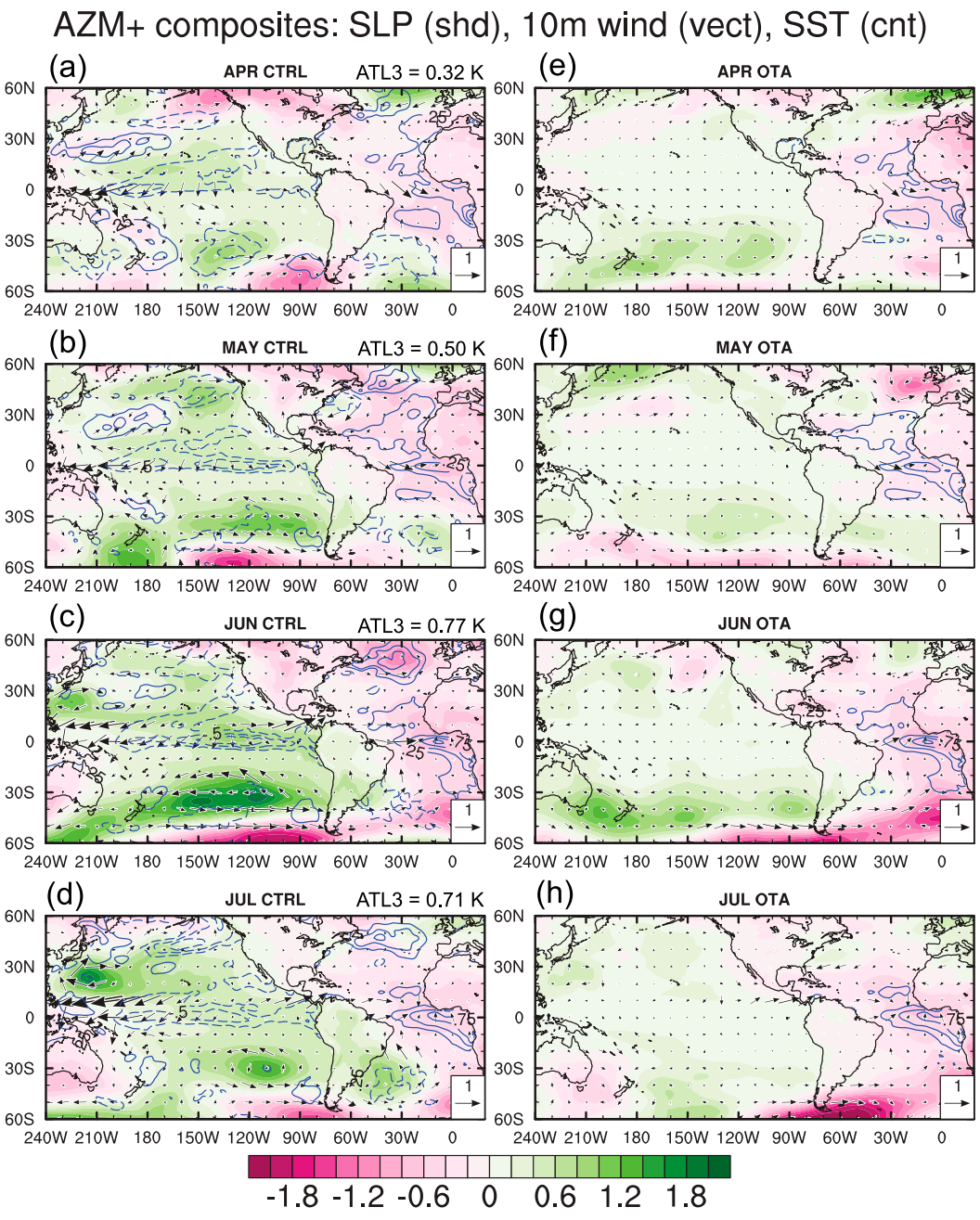

FIG. 4. As in Fig. 3, but for warm AZM events. The value of the ATL3 index is shown on the right above each panel for CTRL.

reproduces the low pressure in the eastern midlatitude Pacific seen in OTA, although some high pressure remains north of 50°N. Thus the partial regression reproduces reasonably well the opposite-signed anomalies of OTA and CTRL in the North Pacific (cf. Fig. 3). An important difference is that the partial regression shows easterly wind anomalies over the eastern equatorial Pacific while OTA does not. This may indicate nonlinearities that are not captured by the partial regression method.

Applying partial regression to the ERA5 reanalysis (Fig. 5a) yields patterns that are roughly similar to those in CTRL (Fig. 5b) but both SLP and wind anomalies tend to have higher amplitude in the reanalysis.

Analysis of the AMIP models (not shown) reveals that, after partial regression, some have anomalous high pressure in the North Pacific (as in CTRL) while others have anomalous low pressure in the region (as in OTA). To examine whether this categorical difference also extends to other regions, we form two ensemble averages based on the sign of AL SLP anomalies. These ensemble averages are shown in Figs. 5c and 5d. The comparison of these two panels does not turn up any

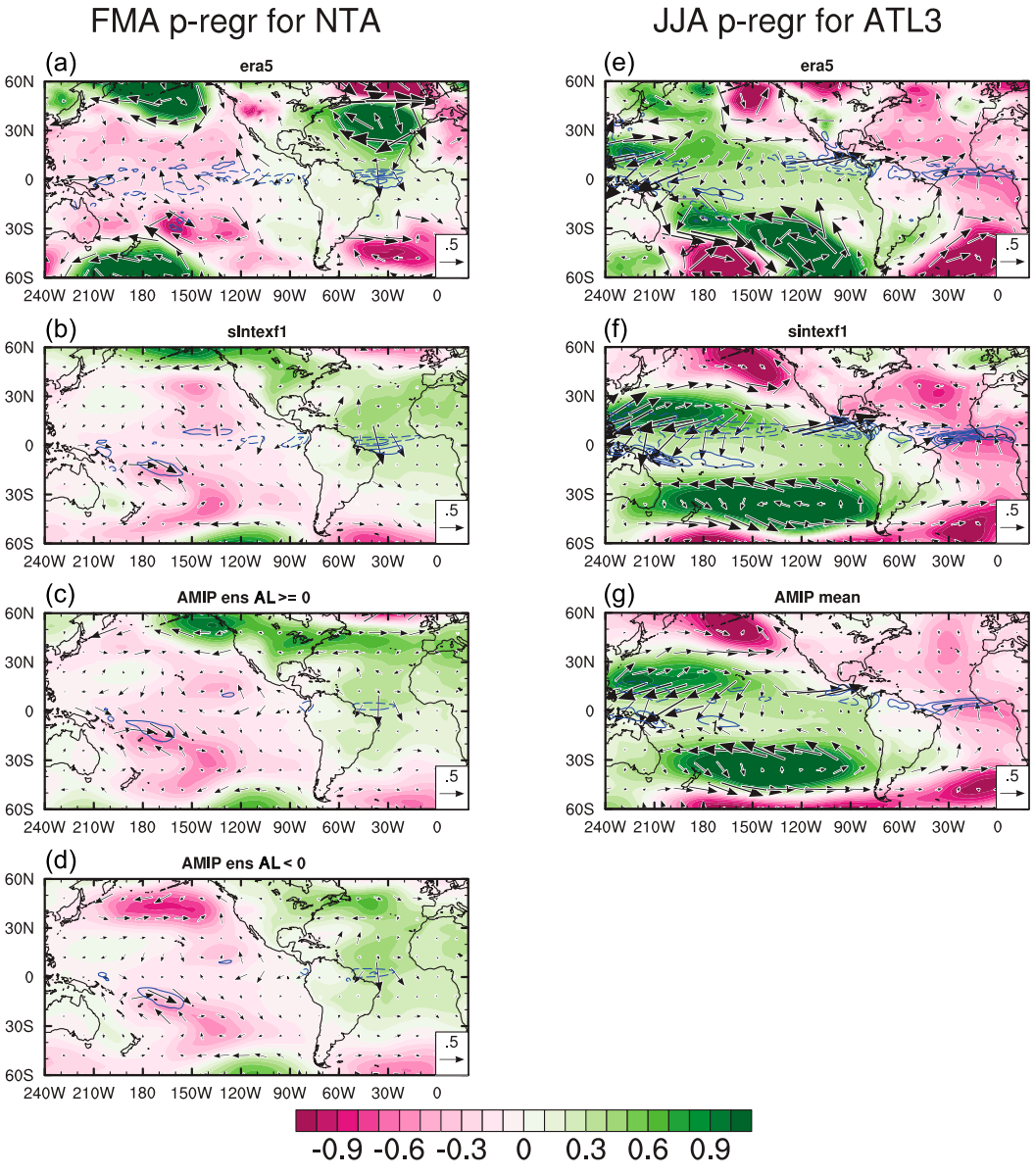

FIG. 5. Partial regression of variables onto the NTA SST index averaged over FMA, after regressing out the Niño-3.4 SST index during the preceding DJF. The regression coefficients shown are SLP (shading; hPa K^{-1}), 10-m wind (vectors; m s^{-1} K^{-1}), and precipitation (contours; interval 1 mm day^{-1} K^{-1}; zero contour omitted; negative contours dashed). The individual panels show (a) ERA5, (b) SINTEX-F CTRL, and the average over AMIP models in which the AL SLP is correlated (c) positively and (d) negatively with the NTA index. Note that the sign has been reversed to facilitate comparison with the composites (Fig. 3). (e)–(g) As in (a)–(d), but for partial regression of variables onto the ATL3 index averaged over JJA, after regressing out the contemporaneous Niño-3.4 SST index; individual panels show ERA5, SINTEX-F CTRL, and the AMIP ensemble mean, respectively.

qualitative differences in other regions. Even in the subtropical North Pacific, just south of the AL region, differences in SLP and 10-m wind are small. Furthermore, both model averages show very good agreement with SINTEX-F CTRL (Fig. 5b) outside of the AL, both qualitatively and quantitatively.

The JJA partial regression patterns for the ATL3 index in ERA5 (Fig. 5e), CTRL (Fig. 5f), and the AMIP ensemble mean (Fig. 5g) agree relatively well with each other. Westerly anomalies are seen over the equatorial Atlantic and the far eastern tropical Pacific, which also agree with the composites of CTRL and OTA (Fig. 4). In other regions of the Pacific, however, the partial regression results are more similar to CTRL (Fig. 4, left) than to OTA (Fig. 4, right). Most notably, there are pronounced easterly anomalies over the western tropical Pacific and westerly anomalies to the north in the subtropics, which are absent in OTA. This suggests that the

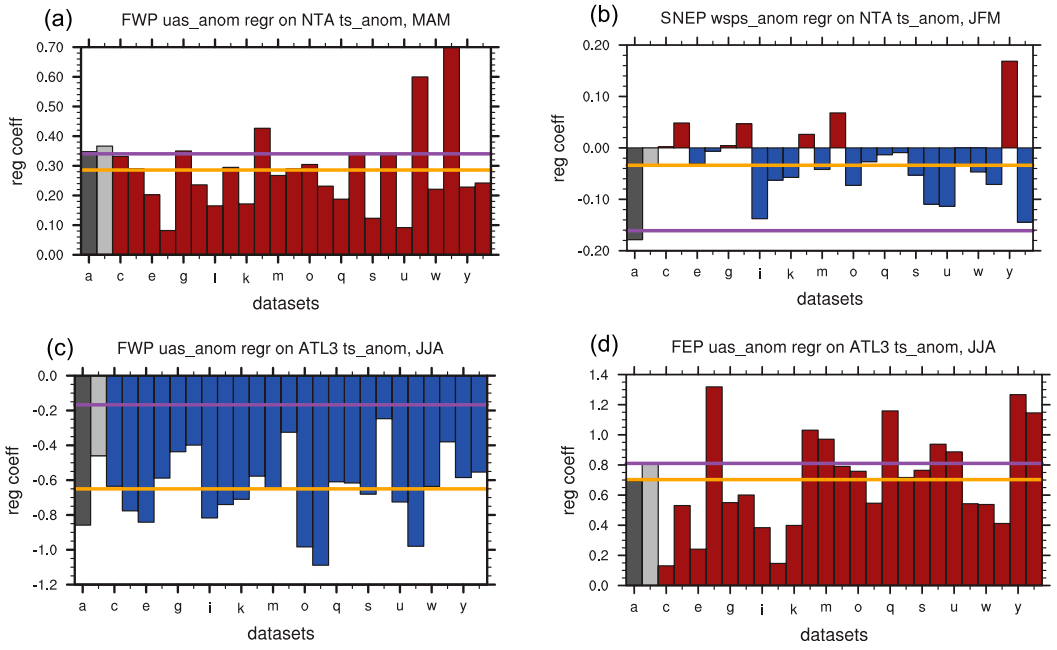

FIG. 6. Partial regression coefficients (calculated as described for Fig. 5 and in section 2; $m\,s^{-1}\,K^{-1}$) for (a) FWP 10-m zonal wind regressed on the NTA SST index and averaged over MAM, (b) SNEP 10-m wind speed regressed on the NTA SST index and averaged over JFM, (c) FWP 10-m zonal wind regressed on the ATL3 SST index and averaged over JJA, and (d) FEP 10-m zonal wind regressed on the ATL3 SST index and averaged over JJA. The *x*-axis labels refer to individual datasets: letter a for ERA5 (dark gray), letter b for CTRL (light gray), and letters c–z for AMIP models (red for positive values, blue for negative values); see Table 2 for the correspondence between letters and AMIP models. The orange horizontal line shows the AMIP ensemble mean. The purple horizontal line shows the value derived from the OTA sensitivity experiment.

partial regression method is not entirely successful in removing the ENSO influence.

We take a closer look at the regression coefficients in individual AMIP models for a few regions of interest (Fig. 6). The partial regression of FWP wind anomalies on NTA SST anomalies for MAM ranges from $0.08\,m\,s^{-1}\,K^{-1}$ (CanESM5) to $0.70\,m\,s^{-1}\,K^{-1}$ (NorESM2-LM) with an average of 0.29. ERA5 and CTRL yield 0.35 and $0.37\,m\,s^{-1}\,K^{-1}$, respectively (Fig. 6a). These values compare reasonably well with the value derived from OTA, which is 0.34.

The influence of the NTA on wind speed in the SNEP region during January–March (JFM) is inconsistent across models (Fig. 6b). While the ERA5 reanalysis, SINTEX-F, and most models show a negative correlation, some models show a positive one. The AMIP ensemble average is $-0.03\,m\,s^{-1}\,K^{-1}$, which is much weaker than the value of $-0.18\,m\,s^{-1}\,K^{-1}$ suggested by the reanalysis or $-0.16\,m\,s^{-1}\,K^{-1}$ suggested by OTA. Given the wide spread across models (Fig. 6b) and the large variability in the SINTEX-F experiments (Fig. S7), confidence in these results is not very high. Consistently, neither the multimodel mean nor the OTA value pass the 95% significance test.

Next, we turn to the equatorial Atlantic. The link between ATL3 SST and FWP zonal wind during boreal summer (JJA) is shown in Fig. 6c. All datasets indicate a negative relation (i.e., warm SST anomalies in the ATL3 are associated with easterly wind anomalies in the FWP region). The sensitivity is $-0.65\,m\,s^{-1}\,K^{-1}$ in the AMIP ensemble average. This is substantially higher than the $-0.17\,m\,s^{-1}\,K^{-1}$ suggested by OTA and may indicate a failure of the partial regression to completely remove the ENSO influence. One potential reason is that, in JJA, there can be remnants of an ENSO event from the preceding DJF but also the onset of an event that peaks in the following DJF (see section 2 of the online supplemental material for more discussion). Deficiencies specific to SINTEX-F could also contribute to the differences between OTA and the AMIP ensemble. The fact that even the partial regression of CTRL disagrees with OTA points to a problem with the partial regression method.

Finally, we examine the link between ATL3 SST and 10-m zonal wind in the far eastern Pacific during JJA (Fig. 6d). Both ERA5 and the AMIP ensemble average suggest a sensitivity of $0.7\,m\,s^{-1}\,K^{-1}$; that is, warm SST anomalies in the ATL3 are associated with westerly wind anomalies in the FEP. The value from OTA ($0.8\,m\,s^{-1}\,K^{-1}$) agrees relatively well with this estimate. OTA also matches the regression-based estimate from SINTEX-F CTRL, although the high level of agreement is likely fortuitous. The robust signal in the FEP is consistent with the OTA composites (Fig. 4).

5. Impact of model biases on the strength of the Atlantic-to-Pacific link

GCMs are subject to systematic errors, and it is an important question to what extent such errors influence our GCM-derived sensitivity estimates. To start, we briefly discuss

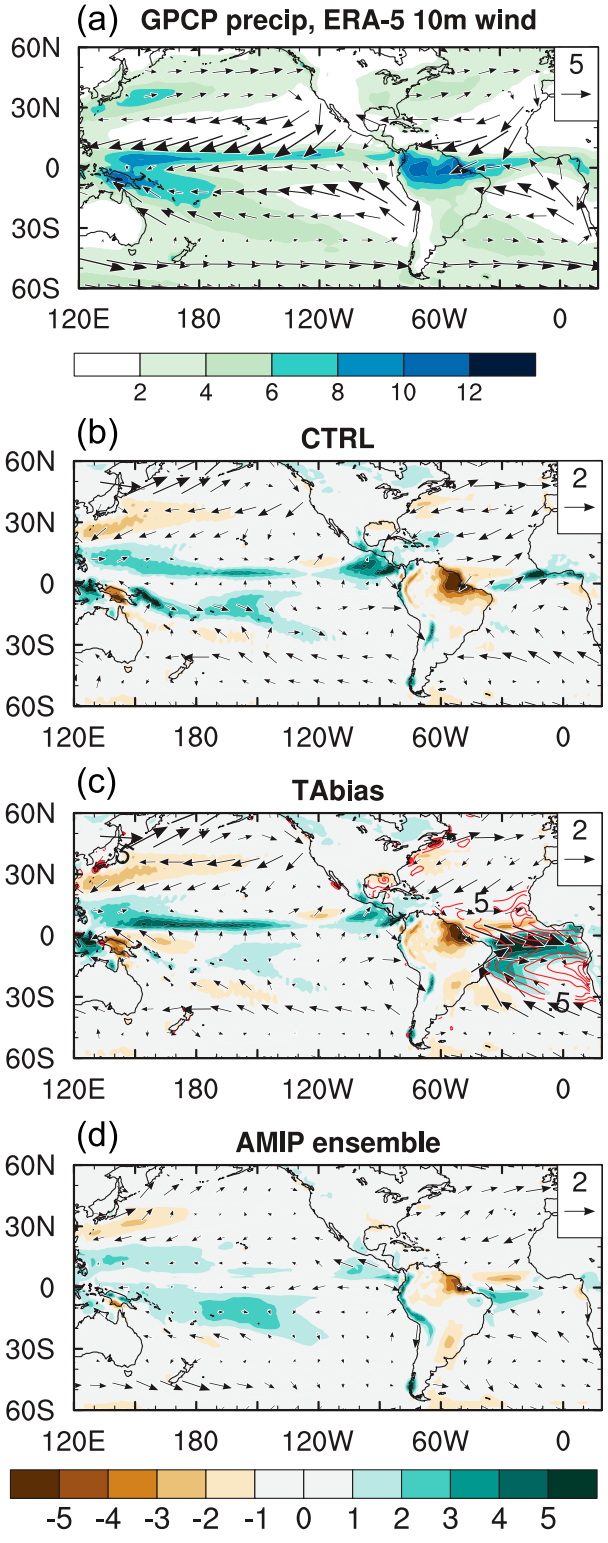

FIG. 7. (a) MAM climatological precipitation from GPCP observations (shading; mm day^{-1}), and 10-m winds from ERA5 reanalysis (vectors; reference 5 m s^{-1}). The bottom three panels show the biases relative to (a) for (b) CTRL, (c) TAbias, and (d) the AMIP ensemble mean. In (b)–(d) the reference vector is 2 m s^{-1}. The red contours in (c) indicate the SST bias relative OISST.

mean state errors in SINTEX-F and the AMIP models during MAM (Fig. 7). A more general discussion of AMIP biases in the tropical Atlantic can be found in Richter and Tokinaga (2020).

The GPCP observations show the Atlantic ITCZ close to the equator, extending westward over the Amazon region (Fig. 7a). Over the equatorial Pacific, high precipitation is found at about 5°N but also south of the equator in the South Pacific convergence zone and extending toward the east. This double ITCZ configuration only occurs in spring, although GCMs produce spurious double ITCZs in other seasons as well (e.g., Li and Xie 2014). The northeast and southeast trades in both basins converge onto the areas of high precipitation.

In SINTEX-F CTRL, a meridional dipole in precipitation biases over the equatorial Atlantic indicates a southward shift of the ITCZ (Fig. 7b). There is also a pronounced dry bias over the Amazon region. These precipitation biases are accompanied by westerly wind biases over the equatorial Atlantic. The AMIP ensemble shows very similar bias patterns in both precipitation and 10-m winds (Fig. 7d). Such biases have been shown to be one of the major reasons for the severe warm SST biases in coupled simulations (e.g., Richter and Xie 2008; Richter et al. 2014). Over the equatorial Pacific, both CTRL and the AMIP ensemble exaggerate the observed double ITCZ pattern.

The SINTEX-F TAbias experiment, with prescribed SST biases, shows exacerbation of the biases seen in CTRL, with both the wet bias south of the equator and the westerly bias on the equator intensifying (Fig. 7c). Interestingly, the tropical Atlantic SST biases also affect the Pacific biases by exacerbating excessive precipitation north of the equator while weakening it to the south.

We repeat the negative NTA composites from section 3 for the TAbias experiment (Fig. 8b) in MAM. The Atlantic response reveals many similarities with CTRL (Fig. 8a), including the southward shift of the ITCZ, northwesterly wind anomalies over the equator, and anomalously high SLP extending from the equator to 50°N. Owing to the warmer mean-state SST in TAbias, however, positive precipitation anomalies extend farther southeastward and are associated with stronger wind and SLP anomalies in the southern tropical Atlantic.

The positive precipitation anomalies in the far western Pacific at 10°N are intensified in TAbias, which is accompanied by a slight strengthening of the westerly wind anomalies north of the equator, and a weakening of the easterly anomalies on the equator. The latter is confirmed by composites of FWP that indicate a weakening of 10-m zonal winds by about 0.2 m s^{-1} (not shown). None of these differences, however, are significant at the 95% level.

The JJA composites of positive AZM events show a few conspicuous differences between CTRL and TAbias (Figs. 8c–f). First, the positive precipitation anomalies are intensified and shifted from the central equatorial Atlantic region toward the southeast in TAbias. This is accompanied by much stronger westerly anomalies on the equator. Furthermore, negative SLP anomalies over the tropical Atlantic strengthen in TAbias,

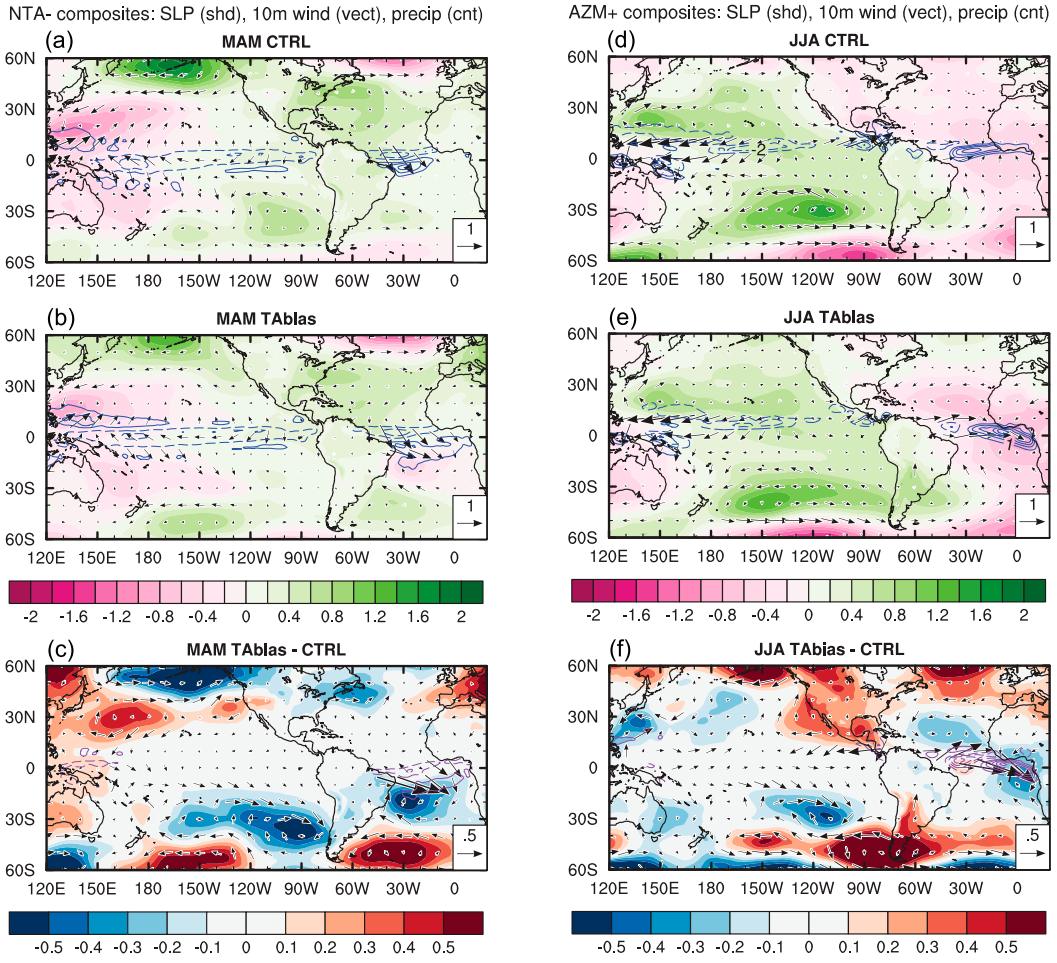

FIG. 8. (a),(b),(d),(e) Anomalies of SLP (shading; hPa), 10-m wind (vectors; reference 1 m s^{-1}), and precipitation (blue contours; contour interval 1 mm day^{-1}; zero -contour omitted; negative contours dashed) composited on cold NTA events and averaged over MAM for CTRL in (a) and Tabias in (b); or composited on warm AZM events and averaged over JJA for CTRL in (d) and Tabias in (e). (c) The difference between (b) and (a). (f) The difference between (e) and (d). In (c) and (f) the contour intervals for SLP and precipitation are 0.1 hPa and 0.5 mm day^{-1}, respectively. The reference vector indicates 0.5 m s^{-1}.

leading to an increase in the interbasin pressure gradient. One might expect this to be accompanied by stronger westerlies in the FEP but the opposite is the case. This appears to be due to the Caribbean SST being about 0.5 K cooler in TAbias, which is enough to inhibit convection (Fig. 8e). Thus it is the regional forcing that seems to dominate the response in the far eastern Pacific. Other differences in the tropical Pacific are small.

An analysis of the AMIP ensemble (Figs. S8 and S9) also suggests a relatively weak influence of model biases on the regression coefficients, except for the FEP during AZM events.

6. Discussion

a. *Putting the results from atmosphere-only simulations into context*

In our analysis we have shown the atmospheric response to tropical Atlantic SST anomalies in atmosphere-only GCM simulations. The general impression from our analysis is that the tropical Atlantic can elicit near-surface wind anomalies on the order of 0.1–0.2 m s^{-1} during the developing phase of ENSO. This may seem weak, but it is important to compare these results with typical ENSO events. Another question left unanswered by the AGCM simulations is whether coupled feedbacks can amplify the initial anomalies into full-fledged ENSO events. While performing dedicated coupled experiments is outside the scope of the present study, we can use observations and AGCM simulations from the CMIP6 archive to put the results from sections 3–5 into context.

We estimated that typical negative NTA events force westerly wind anomalies of about 0.2 m s^{-1} in the FWP during spring. How does this compare to MAM wind anomalies that precede El Niño events? Composites of El Niño Modoki events in CTRL and ERA5 show FWP anomalies of 0.9 and 0.6 m s^{-1}, respectively. This suggests that negative NTA events can contribute roughly 20%–30% of the wind anomalies for an

El Niño Modoki event. The contributions are somewhat smaller for regular El Niño events.

For the influence of negative NTA events on the SNEP during JFM, OTA estimates a wind speed anomaly of $-0.1\,m\,s^{-1}$, while AMIP models disagree on the sign but, on average, estimate around $-0.02\,m\,s^{-1}$. Disagreement on the sign of the NTA influence exists also in the El Niño Modoki composites in CTRL and ERA5, with the former suggesting $-0.04\,m\,s^{-1}$ and the latter $+0.02\,m\,s^{-1}$. The results indicate that, in terms of magnitude, SNEP wind anomalies in OTA and the AMIP models are comparable with those observed during the early developing phase of El Niño Modoki. Given the disagreement on the sign, however, it is clear that these estimates are very uncertain. Larger ensemble sizes would be needed to obtain robust model-based estimates. If our estimates are close to the truth, it would seem that the NTA influence could easily be drowned out by atmospheric internal variability, and that other influences are likely to dominate.

For the influence of positive AZM events on FWP zonal wind anomalies, the AMIP ensemble average suggests roughly $-0.4\,m\,s^{-1}$ (easterly anomalies), while the OTA estimate is only $-0.1\,m\,s^{-1}$. La Niña composites based on CTRL and ERA5 indicate -1.0 and $-1.3\,m\,s^{-1}$, respectively. Thus the OTA sensitivity experiment suggests that the AZM-induced wind anomalies are 10% or less of those seen during typical La Niña events. This would suggest a very limited influence of the equatorial Atlantic on ENSO development. The AMIP models suggest a stronger influence, but their estimates may be systematically biased due to the difficulties associated with removing the ENSO-to-Atlantic influence. An alternative approach for removing the ENSO influence (Figs. S4 and S5) yields a substantially smaller discrepancy between the regression analysis and OTA (although the former estimate is still about twice as large). This suggests that regressing out ENSO-related variability is not trivial and that incomplete removal may lead to overestimates of remote influences on the tropical Pacific.

For the FEP, OTA and the AMIP ensemble roughly agree on zonal wind anomalies of about $0.5\,m\,s^{-1}$ during positive AZM events. This is about 50%–70% of the strength of wind anomalies seen during El Niño events, although it is not clear whether anomalies in this region significantly influence ENSO development.

Overall, the results suggest that the tropical Atlantic can induce wind anomalies over the Pacific that have about 20% the magnitude of those seen during ENSO events. For the northern tropical Atlantic, however, one has to remember that most NTA events are initiated by ENSO itself during winter. As the NTA event matures in the following months, it induces wind anomalies over the tropical Pacific that oppose the ongoing ENSO event. Thus, the NTA influence can be interpreted as a delayed negative feedback that accelerates the decay of ENSO. This is consistent with the results of Dommenget et al. (2006) and Wang et al. (2017), who found that removing the tropical Atlantic feedback in a simple climate model led to a longer ENSO period.

Finally, we note that, when opposite-signed events are considered, the estimates of the Atlantic influence become weaker, indicating that the results presented here are generous estimates.

b. *Reconciliation with previous studies*

H13 was one of the early studies to point at an important influence of the tropical Atlantic on ENSO evolution. Both our sensitivity experiments and partial regressions show patterns that are very similar to their analysis. In addition to partial regression analysis, they also perform coupled GCM experiments in which a positive NTA event is prescribed in the tropical Atlantic, while the coupled model evolves freely elsewhere. In these experiments, an easterly anomaly of about $-0.8\,m\,s^{-1}$ develops in the far western Pacific. This is about 4 times stronger than what our analysis suggests. Their composite NTA SST anomaly, however, is about 3 times stronger than ours and seems to be representative of an extreme event. It is not quite clear why their composite SST anomaly is so much more pronounced than ours, as they use a compositing criterion that is only a little more stringent than ours (1.0 vs 0.8 standard deviations). After accounting for the amplitude of their SST anomalies the results are already quite close to ours. In addition, the GFDL CM2.1 model used in their study tends to produce very strong variability (Delworth et al. 2006), so that it appears that the results of H13 are actually quite compatible with ours, even without considering amplification by coupled feedbacks.

Ding et al. (2012) use a similar GCM experiment but, in addition to the northern tropical Atlantic, they restore SSTs also in the southern tropical Atlantic. Their finding that the tropical Atlantic forcing can explain about 10% of equatorial Pacific SST variability is not entirely inconsistent with our results (although we can only conjecture about SST variability based on the wind variability in our analysis). For the eastern equatorial Pacific, however, they find that SSTs are correlated with observations at more than 0.5 during spring and summer. This is at odds with our sensitivity experiments, but still within the range of the AMIP ensemble (not shown). Thus, inter-model variance may explain the stronger linkage, but more analysis would be needed to confirm this.

By performing a GCM experiment with partial data assimilation in the tropical Atlantic, Chikamoto et al. (2020) found that the tropical Atlantic can explain about 5% of ENSO variability (based on the correlation of 0.22 between the Niño-3.4 index in observations and the sensitivity test). This suggests a smaller contribution than the one found by Ding et al. (2012).

Wang et al. (2017) suggest that the link between NTA SST in MAM and Niño-3.4 SST in the following winter is dependent on the phase of the Atlantic multidecadal oscillation (AMO). They find correlations of about -0.5 and -0.2 for the positive and negative phases of the AMO, respectively. The AMO switched from negative to positive in the mid-1990s and thus our results average over both phases and should lie somewhere between -0.3 and -0.4, which is consistent with a correlation analysis of SINTEX-F output (not shown). We also found a dependence on analysis period but did not investigate this further due to the generally short record.

Finally, Zhang et al. (2021) suggest that the correlations found between the NTA and pursuant ENSO events can be

explained entirely by the autocorrelation of ENSO and the phase-locked nature of these two patterns. While our results suggest that the impact of the tropical Atlantic on ENSO is weak, we do find it to be statistically significant and, because our OTA experiment eliminates ENSO variability, it is not subject to the autocorrelation argument of Zhang et al. (2021).

7. Summary and conclusions

We have investigated the impact of tropical Atlantic SST anomalies on El Niño–Southern Oscillation (ENSO) using sensitivity experiments with prescribed SST configurations, AMIP simulations from the CMIP6 archive, and the ERA5 reanalysis. Our focus has been on the influence of northern tropical Atlantic (NTA) SST anomalies on 10-m zonal winds in the far western Pacific (FWP) and 10-m wind speed in the subtropical northeastern Pacific (SNEP), and on the influence of SST anomalies associated with the equatorial Atlantic zonal mode (AZM) on 10-m zonal winds in the FWP and in the far eastern Pacific (FEP).

Applying composite analysis to the output of the sensitivity experiments, and partial regression analysis to the AMIP ensemble and the ERA5, we find that all datasets agree on the sign and the order of magnitude of the Pacific response to tropical Atlantic SST anomalies. For cold events in the NTA, the atmospheric response over the Pacific during winter and spring consists of westerly winds in the FWP, reduced wind speed in the SNEP, and a deepening of the Aleutian low. The tropical wind anomalies are conducive to the development of El Niño events in the following winter, although their amplitude is only about 20% of those that typically accompany ENSO events. Moreover, SST anomalies in the NTA during spring are mostly the consequence of ENSO events in the preceding fall and winter (Enfield and Mayer 1997). Thus, the NTA influence should be seen as a negative feedback on ENSO rather than an independent forcing of ENSO events.

For the FWP, the sensitivity experiments, AMIP ensemble, and reanalysis all agree remarkably well on the magnitude of the wind anomalies during MAM. This cannot be said of the SNEP during JFM, where the reanalysis and sensitivity experiments suggest a response that is about 4 times stronger than that of the AMIP ensemble, and where some AMIP models disagree on the sign. One reason for the relatively poor agreement is the large internal variability this subtropical region experiences during winter. This is even more evident for the response of the Aleutian low. Larger ensembles would be needed to reduce uncertainty.

For warm AZM events, the sensitivity experiments suggest easterly wind anomalies in the FWP during JJA that are about 10% of those seen during typical La Niña events. Partial regression of AMIP output and the ERA5 reanalysis, on the other hand, suggests a response that is about 3–4 times as strong. Since regressing out the ENSO influence is not expected to be completely effective, we put more confidence into the results from the sensitivity experiments. Furthermore, in attempting to isolate the influence of a particular region (the equatorial Atlantic in this case), the regression analysis may miss destructive interference from other regions of the tropical Atlantic.

For the FEP, all datasets agree on a relatively strong impact from AZM events. The relevance of these wind anomalies to the development of ENSO remains to be verified.

Overall, our results suggest that the tropical Atlantic plays a secondary role in the evolution of ENSO. The role of the NTA is mostly to accelerate the decay of ENSO. The equatorial Atlantic, being less dependent on ENSO, could potentially also help initiating events. AZM events, however, mature in summer, when many ENSO events are already well underway. Thus, the equatorial Atlantic is more likely to modulate ENSO events, by either accelerating or weakening their growth.

Model-based estimates may be affected by biases but in the context of the atmosphere-only simulations examined here they do not appear to be a game changer. Moreover, individual AMIP models come to lie on both sides of the ERA5 reanalysis, indicating that errors are likely to partially cancel out in the ensemble mean.

An important question that we have not answered is how the Pacific wind response examined here might be amplified by coupled ocean–atmosphere processes. This will require dedicated GCM experiments and is beyond the scope of the present study. Particularly the pathway via the SNEP will require large ensembles to filter out the strong atmospheric noise in the region. Several studies have already addressed these questions (e.g., H13; Jiang and Li 2021) but we believe much more work remains to be done. We hope that the insights gained here will be helpful in guiding further studies.

Acknowledgments. This work was supported by Japan Society for the Promotion Science KAKENHI Grants JP18H01281, JP18H03726, JP19H05703, and JP19H05704.

Data availability statement. GPCP data were downloaded from NOAA PSL via https://psl.noaa.gov/data/gridded/data.gpcp.html, ERA5 data from the Copernicus Climate Data Store via https://cds.climate.copernicus.eu/cdsapp#!/dataset/reanalysis-era5-single-levels-monthly-means?tab=form, and the CMIP6 data from the ESGF via https://esgf-node.llnl.gov/projects/cmip6/. The processed SINTEX-F output used to making the plots can be obtained from https://doi.org/10.7910/DVN/ODNDQQ.

REFERENCES

Adler, R. F., and Coauthors, 2003: The version 2 Global Precipitation Climatology Project (GPCP) monthly precipitation analysis (1979–present). *J. Hydrometeor.*, **4**, 1147–1167, https://doi.org/10.1175/1525-7541(2003)004<1147:TVGPCP>2.0.CO;2.

Alexander, M. A., and Coauthors, 2002: The atmospheric bridge: The influence of ENSO teleconnections on air–sea interaction over the global oceans. *J. Climate*, **15**, 2205–2231, https://doi.org/10.1175/1520-0442(2002)015<2205:TABTIO>2.0.CO;2.

Amaya, D. J., 2019: The Pacific Meridional Mode: A review. *Curr. Climate Change Rep.*, **5**, 296–307, https://doi.org/10.1007/s40641-019-00142-x.

——, M. J. DeFlorio, A. J. Miller, and S.-P. Xie, 2017: WES feedback and the Atlantic meridional mode: Observations and CMIP5 comparisons. *Climate Dyn.*, **49**, 1665–1679, https://doi.org/10.1007/s00382-016-3411-1.

Ashok, K., S. K. Behera, S. A. Rao, H. Weng, and T. Yamagata, 2007: El Niño Modoki and its possible teleconnection. *J. Geophys. Res.*, **112**, C11007, https://doi.org/10.1029/2006JC003798.

Bellenger, H., and Coauthors, 2014: ENSO representation in climate models: From CMIP3 to CMIP5. *Climate Dyn.*, **42**, 1999–2018, https://doi.org/10.1007/s00382-013-1783-z.

Cabos, W., A. de la Vara, and S. Koseki, 2019: Tropical Atlantic variability: Observations and modeling. *Atmosphere*, **10**, 502, https://doi.org/10.3390/atmos10090502.

Cai, W., and Coauthors, 2019: Pantropical climate interactions. *Science*, **363**, eaav4236, https://doi.org/10.1126/science.aav4236.

Chang, P., L. Ji, and H. Li, 1997: A decadal climate variation in the tropical Atlantic Ocean from thermodynamic air–sea interactions. *Nature*, **385**, 516–518, https://doi.org/10.1038/385516a0.

——, Y. Fang, R. Saravanan, L. Ji, and H. Seidel, 2006: The cause of the fragile relationship between the Pacific El Niño and the Atlantic Niño. *Nature*, **443**, 324–328, https://doi.org/10.1038/nature05053.

Chiang, J. C. H., and A. H. Sobel, 2002: Tropical tropospheric temperature variations caused by ENSO and their influence on the remote tropical climate. *J. Climate*, **15**, 2616–2631, https://doi.org/10.1175/1520-0442(2002)015<2616:TTTVCB>2.0.CO;2.

——, and D. J. Vimont, 2004: Analogous Pacific and Atlantic meridional modes of tropical atmosphere–ocean variability. *J. Climate*, **17**, 4143–4158, https://doi.org/10.1175/JCLI4953.1.

Chikamoto, Y., Z. F. Johnson, S.-Y. Wang, M. J. McPhaden, and T. Mochizuki, 2020: El Niño–Southern Oscillation evolution modulated by Atlantic forcing. *J. Geophys. Res. Oceans*, **125**, e2020JC016318, https://doi.org/10.1029/2020JC016318..

Covey, D. L., and S. Hastenrath, 1978: The Pacific El Niño phenomenon and the Atlantic circulation. *Mon. Wea. Rev.*, **106**, 1280–1287, https://doi.org/10.1175/1520-0493(1978)106<1280:TPENPA>2.0.CO;2.

Curtis, S., and S. Hastenrath, 1995: Forcing of anomalous sea surface temperature evolution in the tropical Atlantic during Pacific warm events. *J. Geophys. Res.*, **100**, 15 835–15 847, https://doi.org/10.1029/95JC01502.

Delworth, T. L., and Coauthors, 2006: GFDL's CM2 global coupled climate models. Part I: Formulation and simulation characteristics. *J. Climate*, **19**, 643–674, https://doi.org/10.1175/JCLI3629.1.

Ding, H., N. S. Keenlyside, and M. Latif, 2012: Impact of the equatorial Atlantic on the El Niño Southern Oscillation. *Climate Dyn.*, **38**, 1965–1972, https://doi.org/10.1007/s00382-011-1097-y.

Ding, R., and Coauthors, 2017: Linking a sea level pressure anomaly dipole over North America to the central Pacific El Niño. *Climate Dyn.*, **49**, 1321–1339, https://doi.org/10.1007/s00382-016-3389-8.

Doi, T., G. A. Vecchi, A. J. Rosati, and T. L. Delworth, 2012: Biases in the Atlantic ITCZ in seasonal–interannual variations for a coarse- and a high-resolution coupled climate model. *J. Climate*, **25**, 5494–5511, https://doi.org/10.1175/JCLI-D-11-00360.1.

Dommenget, D., V. Semenov, and M. Latif, 2006: Impacts of the tropical Indian and Atlantic Oceans on ENSO. *Geophys. Res. Lett.*, **33**, L11701, https://doi.org/10.1029/2006GL025871.

Enfield, D. B., and D. A. Mayer, 1997: Tropical Atlantic sea surface temperature variability and its relation to El Niño–Southern Oscillation. *J. Geophys. Res.*, **102**, 929–945, https://doi.org/10.1029/96JC03296.

Frauen, C., and D. Dommenget, 2012: Influences of the tropical Indian and Atlantic Oceans on the predictability of ENSO. *Geophys. Res. Lett.*, **39**, L02706, https://doi.org/10.1029/2011GL050520.

Gill, A. E., 1980: Some simple solutions for heat-induced tropical circulation. *Quart. J. Roy. Meteor. Soc.*, **106**, 447–462, https://doi.org/10.1002/qj.49710644905.

Gualdi, S., A. Navarra, E. Guilyardi, and P. Delecluse, 2003: Assessment of the tropical Indo-Pacific climate in the SINTEX CGCM. *Ann. Geophys.*, **46**, 1–26, https://doi.org/10.4401/ag-3385.

Ham, Y.-G., J.-S. Kug, J.-Y. Park, and F.-F. Jin, 2013a: Sea surface temperature in the north tropical Atlantic as a trigger for El Niño/Southern Oscillation events. *Nat. Geosci.*, **6**, 112–116, https://doi.org/10.1038/ngeo1686.

——, ——, and ——, 2013b: Two distinct roles of Atlantic SSTs in ENSO variability: North tropical Atlantic SST and Atlantic Niño. *Geophys. Res. Lett.*, **40**, 4012–4017, https://doi.org/10.1002/grl.50729.

Hastenrath, S., and L. Heller, 1977: Dynamics of climatic hazards in northeast Brazil. *Quart. J. Roy. Meteor. Soc.*, **103**, 77–92, https://doi.org/10.1002/qj.49710343505.

Hersbach, H., and Coauthors, 2018: Operational global reanalysis: Progress, future directions and synergies with NWP. ERA Rep. Series 27, 63 pp., https://www.ecmwf.int/node/18765.

Huang, B., 2004: Remotely forced variability in the tropical Atlantic Ocean. *Climate Dyn.*, **23**, 133–152, https://doi.org/10.1007/s00382-004-0443-8.

Jansen, M. F., D. Dommenget, and N. Keenlyside, 2009: Tropical atmosphere–ocean interactions in a conceptual framework. *J. Climate*, **22**, 550–567, https://doi.org/10.1175/2008JCLI2243.1.

Jiang, L., and T. Li, 2021: Impacts of tropical North Atlantic and equatorial Atlantic SST Anomalies on ENSO. *J. Climate*, **34**, 5635–5655, https://doi.org/10.1175/JCLI-D-20-0835.1.

Kataoka, T., M. Kimoto, M. Watanabe, and H. Tatebe, 2019: Wind–mixed layer–SST feedbacks in a tropical air–sea coupled system: Application to the Atlantic. *J. Climate*, **32**, 3865–3881, https://doi.org/10.1175/JCLI-D-18-0728.1.

Klein, S. A., B. J. Soden, and N. C. Lau, 1999: Remote sea surface temperature variations during ENSO: Evidence for a tropical atmospheric bridge. *J. Climate*, **12**, 917–932, https://doi.org/10.1175/1520-0442(1999)012<0917:RSSTVD>2.0.CO;2.

Kucharski, F., I.-S. Kang, R. Farneti, and L. Feudale, 2011: Tropical Pacific response to 20th century Atlantic warming. *Geophys. Res. Lett.*, **38**, L03702, https://doi.org/10.1029/2010GL046248.

——, and Coauthors, 2015: Tropical Atlantic influence on Pacific variability and mean state in the twentieth century in observations and CMIP5. *Climate Dyn.*, **44**, 881–896, https://doi.org/10.1007/s00382-014-2228-z.

Lee, S.-K., D. B. Enfield, and C. Wang, 2008: Why do some El Niños have no impact on tropical North Atlantic SST? *Geophys. Res. Lett.*, **35**, L16705, https://doi.org/10.1029/2008GL034734.

Li, G., and S.-P. Xie, 2014: Tropical biases in CMIP5 multimodel ensemble: The excessive equatorial Pacific cold tongue and double ITCZ problems. *J. Climate*, **27**, 1765–1780, https://doi.org/10.1175/JCLI-D-13-00337.1.

Lübbecke, J. F., and M. J. McPhaden, 2012: On the inconsistent relationship between Pacific and Atlantic Niños. *J. Climate*, **25**, 4294–4303, https://doi.org/10.1175/JCLI-D-11-00553.1.

——, B. Rodríguez-Fonseca, I. Richter, M. Martín-Rey Marta, T. Losada, I. Polo, and N. S. Keenlyside, 2018: Equatorial Atlantic variability—Modes, mechanisms, and global teleconnections. *Wiley Interdiscip. Rev.: Climate Change*, **9**, e527, https://doi.org/10.1002/wcc.527.

Luo, J.-J., S. Masson, S. K. Behera, P. Delecluse, S. Gualdi, A. Navarra, and T. Yamagata, 2003: South Pacific origin of the decadal ENSO-like variation as simulated by a coupled GCM. *Geophys. Res. Lett.*, **30**, 2250, https://doi.org/10.1029/2003GL018649.

——, ——, E. Roeckner, G. Madec, and T. Yamagata, 2005: Reducing climatology bias in an ocean–atmosphere OGCM

with improved coupling physics. *J. Climate*, **18**, 2344–2360, https://doi.org/10.1175/JCLI3404.1.

Madec, G., P. Delecluse, M. Imbard, and C. Levy, 1998: *OPA 8.1 Ocean General Circulation Model Reference Manual*. Note du Pôle de modélisation 11, IPSL, 91 pp.

Matsuno, T., 1966: Quasi-geostrophic motion in the equatorial area. *J. Meteor. Soc. Japan*, **44**, 25–43, https://doi.org/10.2151/jmsj1965.44.1_25.

Polo, I., and Coauthors, 2015: Processes in the Pacific La Niña onset triggered by the Atlantic Niño. *Climate Dyn.*, **44**, 115–131, https://doi.org/10.1007/s00382-014-2354-7.

Reynolds, R. W., N. A. Rayner, T. M. Smith, D. C. Stokes, and W. Wang, 2002: An improved in situ and satellite SST analysis for climate. *J. Climate*, **15**, 1609–1625, https://doi.org/10.1175/1520-0442(2002)015<1609:AIISAS>2.0.CO;2.

Richter, I., and S.-P. Xie, 2008: On the origin of equatorial Atlantic biases in coupled general circulation models. *Climate Dyn.*, **31**, 587–598, https://doi.org/10.1007/s00382-008-0364-z.

——, and T. Doi, 2019: Estimating the role of SST in atmospheric surface wind variability over the tropical Atlantic and Pacific. *J. Climate*, **32**, 3899–3915, https://doi.org/10.1175/JCLI-D-18-0468.1.

——, and H. Tokinaga, 2020: An overview of the performance of CMIP6 models in the tropical Atlantic: Mean state, variability, and remote impacts. *Climate Dyn.*, **55**, 2579–2601, https://doi.org/10.1007/s00382-020-05409-w.

——, and ——, 2021: The Atlantic Niño: Dynamics, thermodynamics, and teleconnections. *Tropical and Extra-Tropical Air–Sea Interactions*, S. K. Behera, Ed., Elsevier, 171–206.

——, S.-P. Xie, S. K. Behera, T. Doi, and Y. Masumoto, 2014: Equatorial Atlantic variability and its relation to mean state biases in CMIP5. *Climate Dyn.*, **42**, 171–188, https://doi.org/10.1007/s00382-012-1624-5.

——, T. Doi, S. K. Behera, and N. Keenlyside, 2018: On the link between mean state biases and prediction skill in the tropics: An atmospheric perspective. *Climate Dyn.*, **50**, 3355–3374, https://doi.org/10.1007/s00382-017-3809-4.

Rodríguez-Fonseca, B., and Coauthors, 2009: Are Atlantic Niños enhancing Pacific ENSO events in recent decades? *Geophys. Res. Lett.*, **36**, L20705, https://doi.org/10.1029/2009GL040048.

Roeckner, E., and Coauthors, 1996: The atmospheric general circulation model ECHAM-4: Model description and simulation of present-day climate. Max-Planck-Institute for Meteorology Rep. 218, 90 pp., http://www.mpimet.mpg.de/fileadmin/publikationen/Reports/MPI-Report_218.pdf.

Saravanan, R., and P. Chang, 2000: Interaction between tropical Atlantic variability and El Niño–Southern Oscillation. *J. Climate*, **13**, 2177–2194, https://doi.org/10.1175/1520-0442(2000)013<2177:IBTAVA>2.0.CO;2.

Sasaki, W., T. Doi, K. J. Richard, and Y. Masumoto, 2014: Impact of the equatorial Atlantic sea surface temperature on the tropical Pacific in a CGCM. *Climate Dyn.*, **43**, 2539–2552, https://doi.org/10.1007/s00382-014-2072-1.

Tokinaga, H., I. Richter, and Y. Kosaka, 2019: ENSO influence on the Atlantic Niño, revisited: Multi-year versus single-year ENSO events. *J. Climate*, **32**, 4585–4600, https://doi.org/10.1175/JCLI-D-18-0683.1.

Valcke, S., L. Terray, and A. Piacentini, 2000: The OASIS coupler user guide version 2.4. Tech. Rep. TR/CGMC/00-10, CERFACS, 85 pp.

Vallès-Casanova, I., S.-K. Lee, G. R. Foltz, and J. L. Pelegri, 2020: On the spatiotemporal diversity of Atlantic Niño and associated rainfall variability over West Africa and South America. *Geophys. Res. Lett.*, **47**, e2020GL087108, https://doi.org/10.1029/2020GL087108.

Wallace, J. M., and D. S. Gutzler, 1981: Teleconnections in the geopotential height field during the Northern Hemisphere winter. *Mon. Wea. Rev.*, **109**, 784–812, https://doi.org/10.1175/1520-0493(1981)109<0784:TITGHF>2.0.CO;2.

Wang, C., 2002: Atmospheric circulation cells associated with the El Niño–Southern Oscillation. *J. Climate*, **15**, 399–419, https://doi.org/10.1175/1520-0442(2002)015<0399:ACCAWT>2.0.CO;2.

——, 2006: An overlooked feature of tropical climate: Inter-Pacific-Atlantic variability. *Geophys. Res. Lett.*, **33**, L12702, https://doi.org/10.1029/2006GL026324.

——, 2019: Three-ocean interactions and climate variability: A review and perspective. *Climate Dyn.*, **53**, 5119–5136, https://doi.org/10.1007/s00382-019-04930-x.

——, S. K. Lee, and C. R. Mechoso, 2010: Inter-hemispheric influence of the Atlantic warm pool on the southeastern Pacific. *J. Climate*, **23**, 404–418, https://doi.org/10.1175/2009JCLI3127.1.

Wang, L., J.-Y. Yu, and H. Paek, 2017: Enhanced biennial variability in the Pacific due to Atlantic capacitor effect. *Nat. Commun.*, **8**, 14887, https://doi.org/10.1038/ncomms14887.

Xie, S.-P., 1996: Westward propagation of latitudinal asymmetry in a coupled ocean–atmosphere model. *J. Atmos. Sci.*, **53**, 3236–3250, https://doi.org/10.1175/1520-0469(1996)053<3236:WPOLAI>2.0.CO;2.

Zhang, W., F. Jiang, M. F. Stuecker, F.-F. Jin, and A. Timmermann, 2021: Spurious North Tropical Atlantic precursors to El Niño. *Nat. Commun.*, **12**, 3096, https://doi.org/10.1038/s41467-021-23411-6.